esa

→ EARTH OBSERVATION SUMMER SCHOOL

Earth System Monitoring & Modelling

30 July–10 August 2018 | ESA–ESRIN | Frascati (Rome) Italy

OCEAN CIRCULATION III

Marie-Hélène RIO

Wednesday: Introduction

- ❑ The different components of the ocean circulation
- ❑ How to estimate (part of) the ocean circulation
  - ✓ from oceanographic in-situ measurements
  - ✓ from space

Thursday: Space and in-situ data synergy for a better retrieval of the ocean circulation

- ❑ Altimetry, geoid, drifters, hydrological profiles for estimating the ocean mean circulation
- ❑ Altimetry, drifters, scatterometers for estimating the Ekman currents
- ❑ SSH/SST synergy for higher resolution surface currents

Friday: The 3D perspective

- ❑ The thermohaline circulation
- ❑ Reconstruction of the 3D horizontal ocean circulation from observations
- ❑ Estimation of the vertical velocity component

Conveyor belt, meridional overturning circulation…

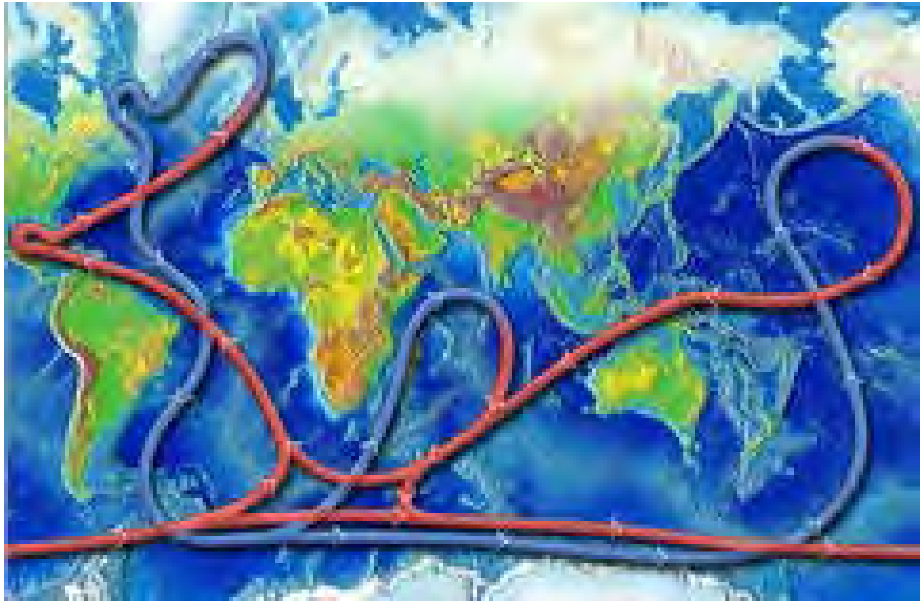

The global ocean circulation connects water masses of the different ocean basins, inducing a large-scale redistribution of heat, carbon and other passive tracers.

The upwelling branch of the thermohaline circulation is important for the ocean's biota as it brings nutrient-rich deep water up to the surface.

The thermohaline circulation is an important factor in the Earth's climate because it transports roughly 10^{15}W of heat poleward into high latitudes, about one quarter of the total heat transport of the ocean/atmosphere circulation system.

~1000 years to close the loop

The thermohaline circulation

The thermohaline circulation consists of:

- Deep water formation: It takes place in a few localised areas: the Greenland-Norwegian Sea, the Labrador Sea, the Mediteranean Sea, the Wedell Sea, the Ross Sea
- Spreading of deep waters (eg, North Atlantic Deep Water , NADW, and Antarctic Bottom Water , AABW), mainly as deep western boundary currents (DWBC).
- Upwelling of deep waters. It is thought to take place mainly in the Antarctic Circumpolar Current region, possibly aided by the wind (Ekman divergence).
- Near-surface currents : these are required to close the flow. In the Atlantic, the surface currents compensating the outflow of NADW range from the Benguela Current off South Africa via Gulf Stream and North Atlantic Current into the Nordic Seas off Scandinavia

The thermohaline circulation

Classical thinking is that thermohaline circulation is driven by global density gradients created by surface heat and freshwater fluxes.
However, the wind forcing, eddy stirring and internal mixing also play a critical role in providing the mechanical forcing needed to maintain a substantial thermohaline circulation.
Three schools of theory for the thermohaline circulation.

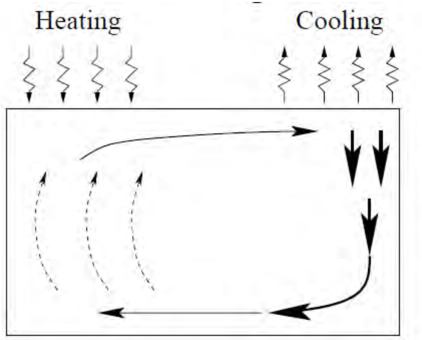

a) Pushing by Deepwater Formation

Surface cooling and ice formation produce dense water that sinks to the great depth.

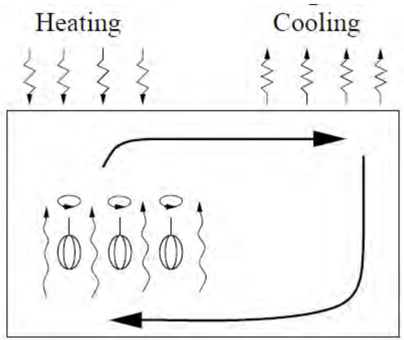

b) Pulling by Deep Mixing

Deep mixing transforms cold water in the deep ocean into warm water, creating room for newly formed deepwater and thus pulling the thermohaline circulation

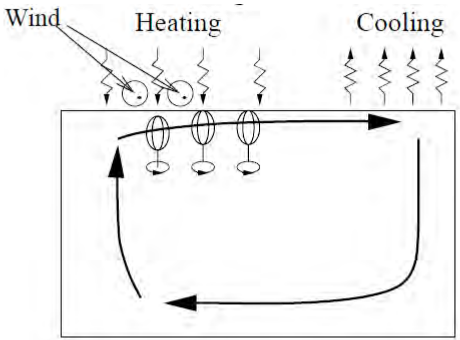

c) Pulling by Wind Stress

Due to the strong upwelling in the Southern Ocean, North Atlantic Deep Water (NADW) is pulling up to the upper ocean

The thermohaline circulation

The AMOC: Atlantic Meridional Overturning Circulation

Relatively warm surface waters from the equator (red) mix with cold, salty water from the north and sink to the ocean floor (blue). This conveyor belt of ocean water maintains the delivery of warm water and weather to the northeast USA and northwest Europe.

Big concern that global warming could provoke a shutdown or a slowing down of the THC in general and the AMOC in particular.

More likely than a breakdown of the THC, which only occurs in very pessimistic scenarios, a weakening of the THC by 20-50%, is simulated by many coupled climate models

Illustration: S. Rahmstorf (Nature 1997)

The thermohaline circulation

Rahmstorf et al, 2015 Nature Climate Change

AMOC index based on surface temperature

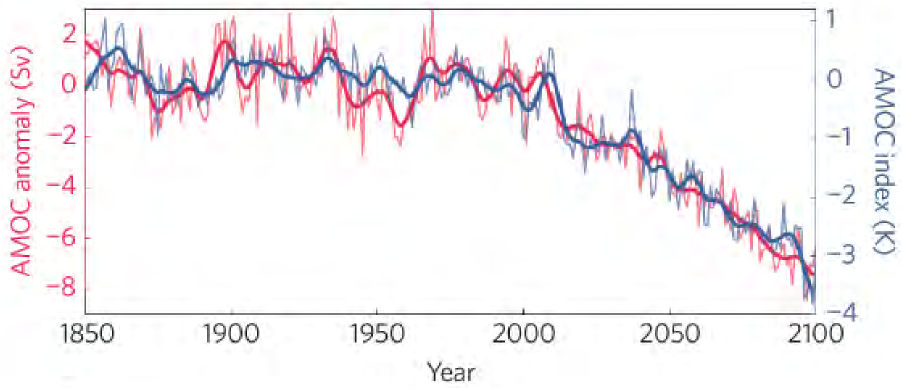

Thornalley *et al.* 2018 provide a longer-term perspective on changes in AMOC strength during the past 1,600 years using a proxy measurement of deep-sea sediment cores that reflects the speeds of the bottom waters that flow along the path of the North Atlantic Deep Water, the deep-water return flow of the AMOC.
They estimate that the AMOC declined in strength by about 15% during the industrial era, relative to its flow in the preceding 1,500 years

Caesar et al, Nature 2018: weakening of the AMOC by about 3 ± 1 sverdrups (around 15%) since the mid-twentieth century analyzing temperature anomalies in the North Atlantic subpolar gyre

- However, the thermohaline circulation mechanisms are very complex and still not fully understood.
- In addition there is a lack of direct observations of the THC

Measuring the AMOC: the RAPID MOC mooring array

An estimate of the meridional flow relating to the MOC along 26.5°N is obtained by decomposing it into three components:

- transport through the Florida Straits
- flow induced by the interaction between wind and the ocean surface (Ekman transport)
- transport related to the difference in sea water density between the American and African continents

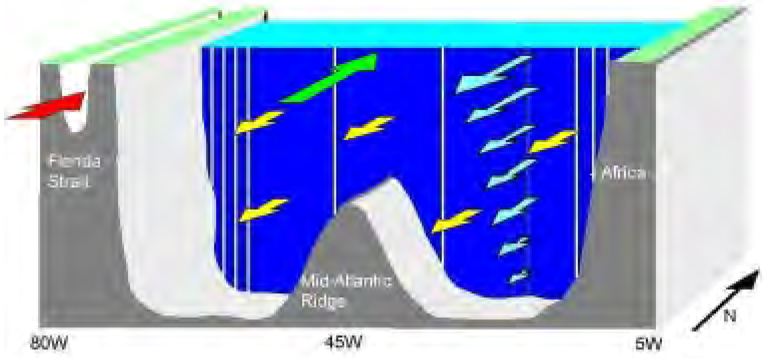

- Since 1982 the Florida current transport is monitored using a submarine cable and snapshot estimates made by shipboard instruments.
- Ekman transport is calculated from wind stress data
- Since 2004, the RAPID MOC mooring array has been deployed to measure vertical profiles of seawater density at a series of different longitudes between the Bahamas and the African continent. The differences in these measured density profiles allows to estimate the current velocities at 26.5°N

Measuring the AMOC: the RAPID array

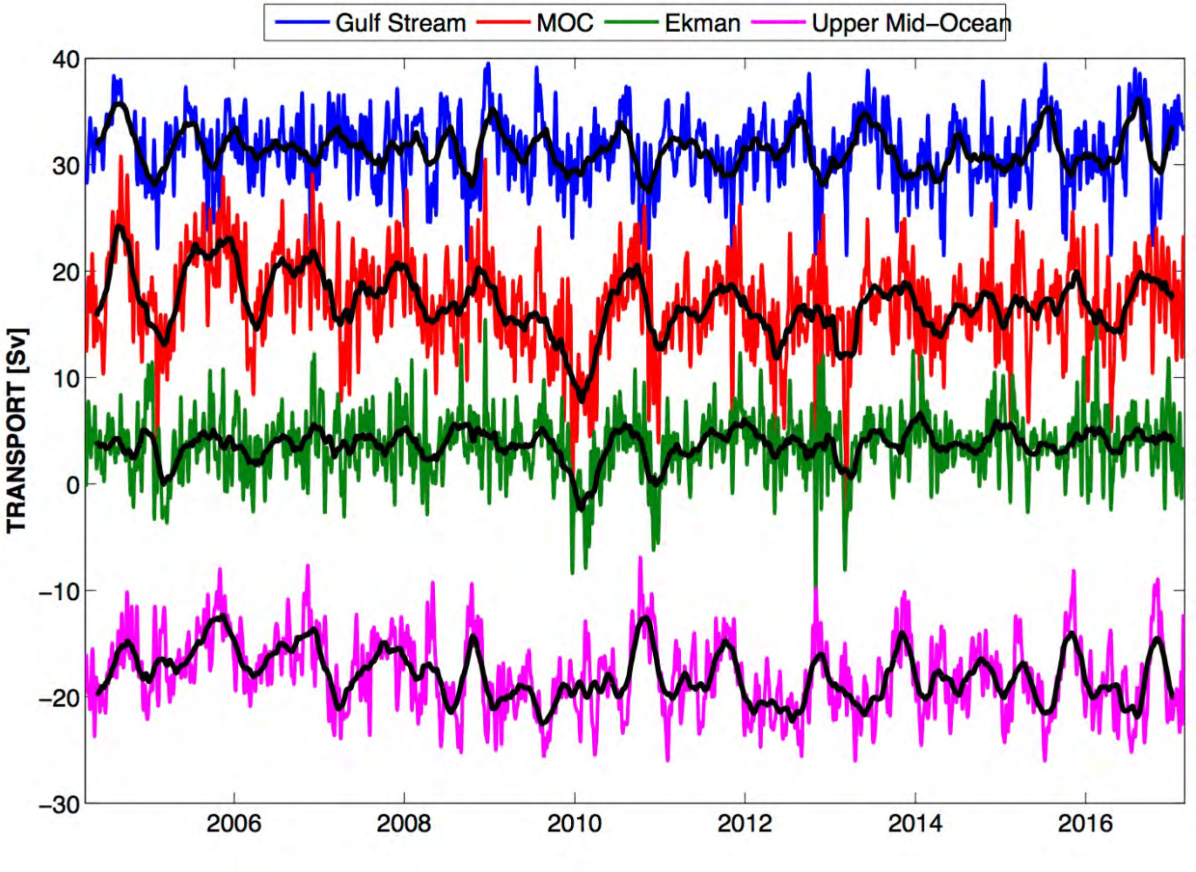

Space and in-situ Observation network

Space data

GOCE, GRACE

Geoid

ERS, ENVISAT,CRYOSAT, SENTINEL-3
TOPEX, JASON

Sea Surface Height

ENVISAT, Sentinel-1

SAR doppler velocity

In-situ data

SVP drifting buoys

Surface/sub-surface velocities

Argo floats

Temperature, salinity profiles

ENVISAT, Sentinel-3

Sea Surface Temperature

ASCAT, QuickScat

Wind speed

Can we estimate the 3D ocean state from our observing system?

Satellite -> observe the ocean surface only
In-situ data can provide information at depth but they are sparse in time and space

- ❑ synthesis can be done through modelling and assimilation systems
- ❑ or 3D reconstruction through statistical observation analysis

3D reconstruction of the geostrophic currents from the thermal wind equation: the SURCOUF3D product (Mulet et al, 2014)

Altimetry :

Field of absolute geostrophic surface currents - weekly - 1/4°

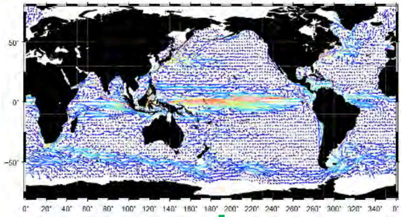

The thermal wind equation

$$u(z=z_i) = u(z=0) + \frac{g}{\rho f}\int_{z=0}^{z_i} \frac{\partial}{\partial y}\rho'(z)\,dz$$

$$v(z=z_i) = v(z=0) - \frac{g}{\rho f}\int_{z=0}^{z_i} \frac{\partial}{\partial x}\rho'(z)\,dz$$

3D gridded T/S field needed
Observing systems:

- Global surface T/S from space data
- Sparse T/S profiles from in-situ data (Argo floats, CTD)

3D reconstruction is needed

- Multiple linear regression method (Guinehut et al, 2012) - CMEMS ARMOR-3D
- M-EOF reconstruction (Buongiorno et al, 2005, 2006, 2012, 2013)
- GEM (Gravest Empirical Mode) in the Southern Ocean (Meijers et al, 2011)

3D reconstruction of the T/S field

ARMOR3D (Guinehut et al, 2012)

SLA

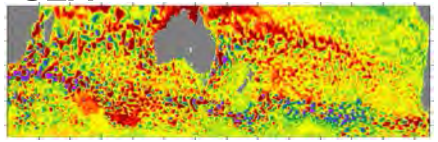

SST

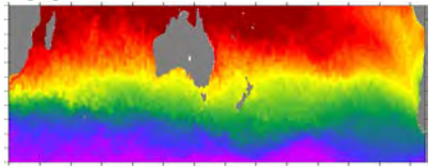

SSS

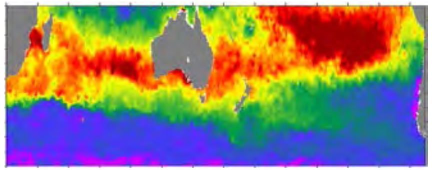

multiple linear regression

T = a ΔSLA + b ΔSST' + Tclim
S = c ΔSLA + d ΔSSS' + Sclim

Climatology T/S (WOA13)

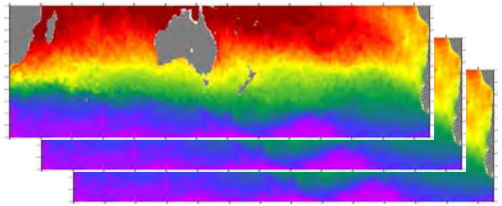

Synthetic T/S

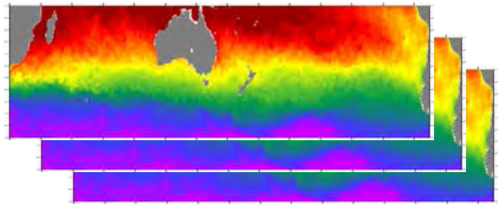

➔ Provides the mesoscale part of the signal

ARMOR3D (Guinehut et al, 2012)

SLA

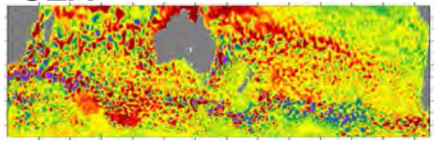

SST

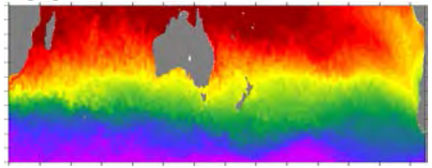

SSS

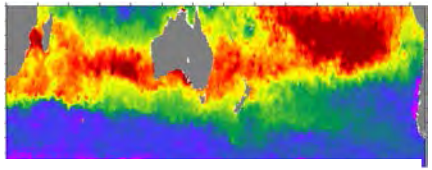

In-situ observations

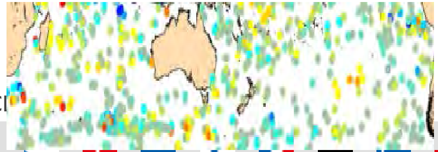

Climatology T/S (WOA13)

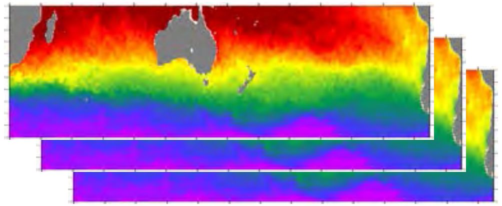

multiple linear regression

T = a ΔSLA + b ΔSST' + Tclim
S = c ΔSLA + d ΔSSS' + Sclim

Synthetic T/S

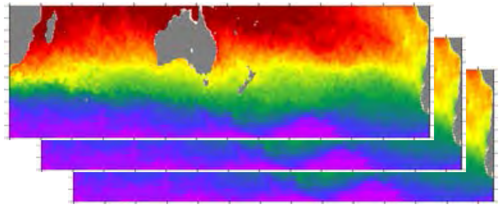

2 optimal interpolation

Combined T/S

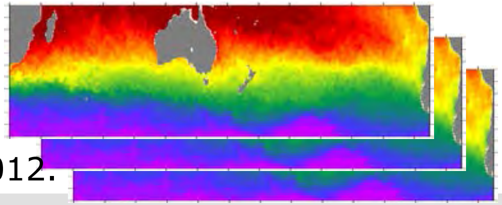

Guinehut S. et al., *JMS* 2004.
Guinehut S. et al., *Ocean Sci*.2012.
Mulet S. et al. *DSR*, 2012.

3D reconstruction of the T/S field

Regression coefficient between SLA and DHA computed using a 1500m depth reference level

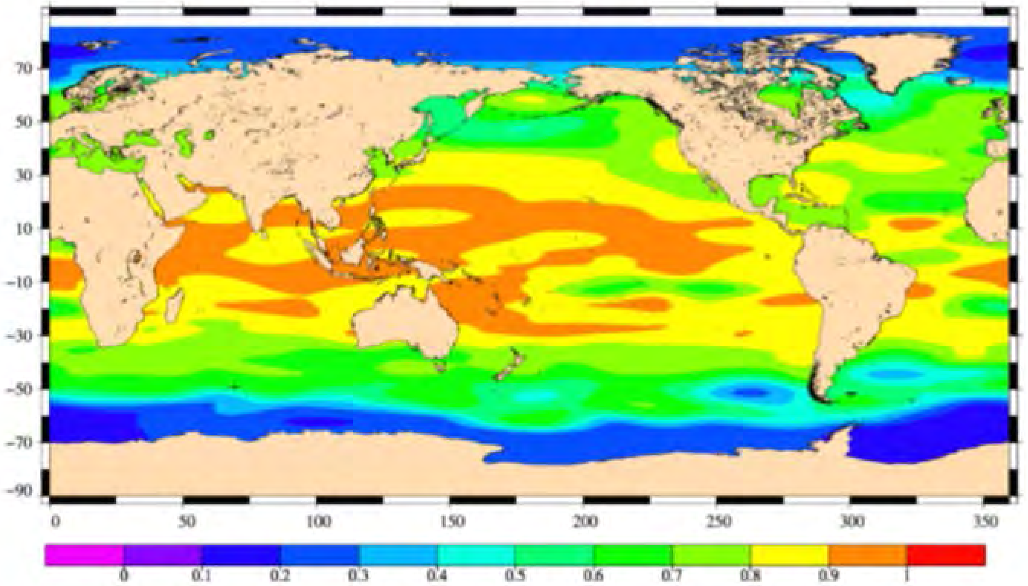

3D reconstruction of the T / S field

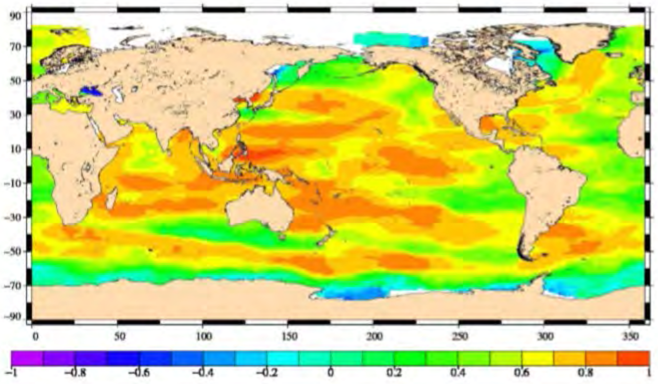

Fig. 1. Annual correlation coefficient between dynamic heights (DH) computed using a reference level at 1500 m depth and temperature (T) field at 100 m depth. The color scale ranges from −1 to 1, every 0.1.

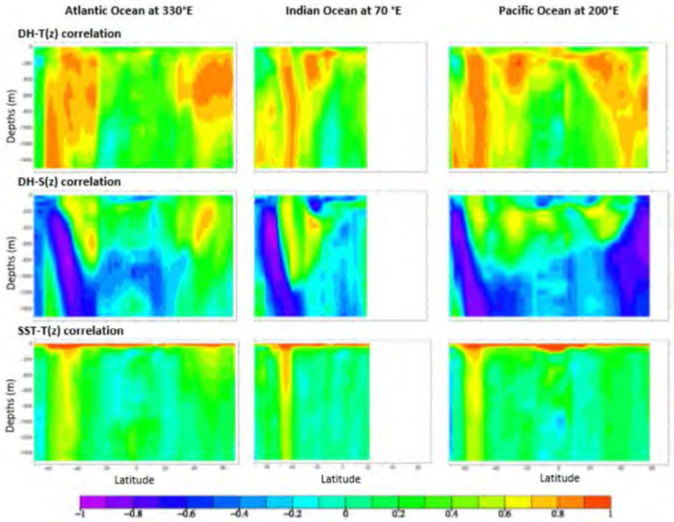

Fig. 2. DH-$T(z)$, DH-$S(z)$ and SST-$T(z)$ annual correlation coefficients for three zonal sections: at 330° E in the Atlantic Ocean, at 70° E in the Indian Ocean and at 200° E in the Pacific Ocean. The latitudes range from 70° S to 70° N for the Atlantic and Pacific Oceans and from 70° S to 30° N for the Indian Ocean and the depths from 0 to −1500 m. The color scale ranges from −1 to 1, every 0.1.

3D reconstruction of the T/S field

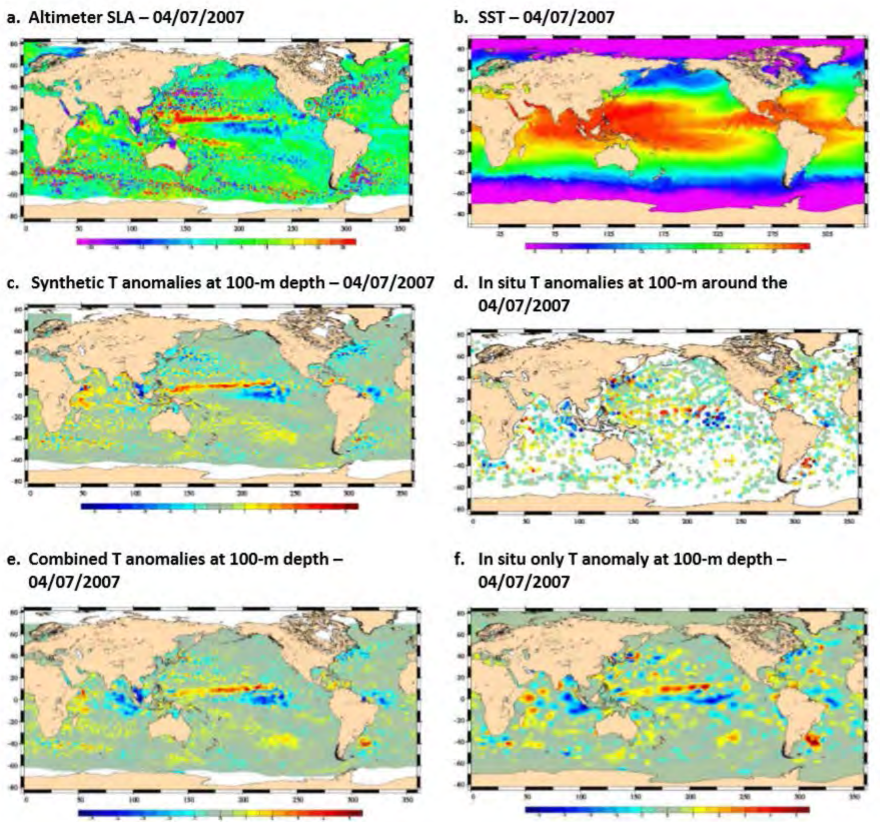

ARMOR3D Validation

Temperature

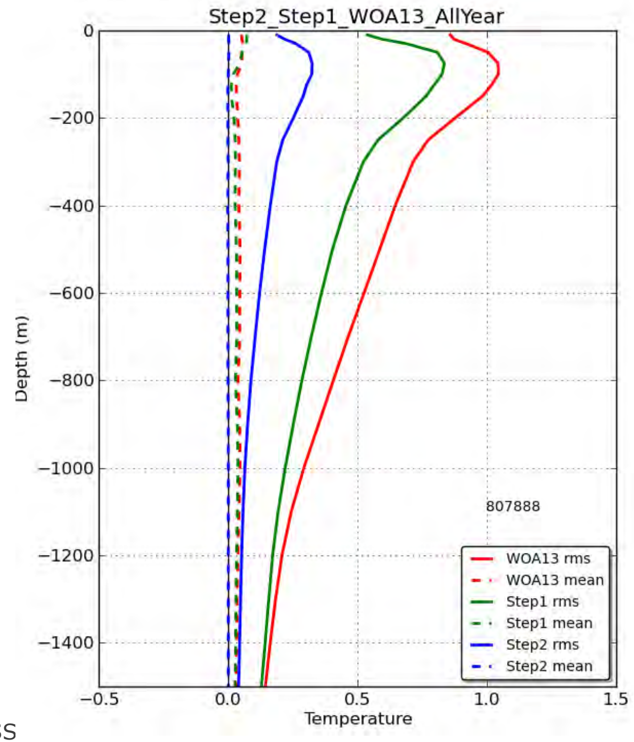

Salinity

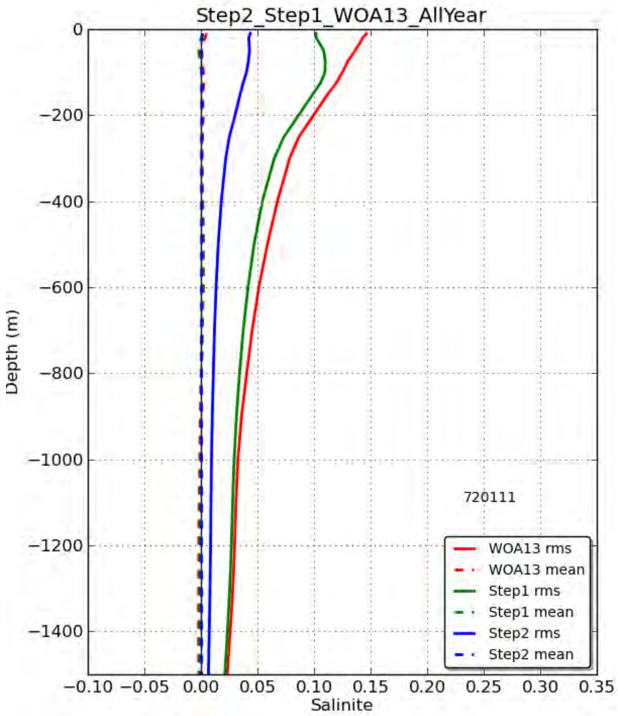

Multivariate Empirical Orthogonal Function Reconstruction

→in situ profiles used to estimate multivariate EOF (T,S,DH)
→Multivariate EOFs used to extrapolate deep values from surface SST, SSS, ADT

mEOF decomposition

$$T(z,t)=\sum_{k=1}^{n} a_k(t)L_k(z)$$
$$S(z,t)=\sum_{k=1}^{n} a_k(t)M_k(z)$$
$$SH(z,t)=\sum_{k=1}^{n} a_k(t)N_k(z)$$

Core of mEOF-R method

$$\boxed{\begin{cases} a_1(t)L_1(0)+a_2(t)L_2(0)+a_3(t)L_3(0)=T(0,t) \\ a_1(t)M_1(0)+a_2(t)M_2(0)+a_3(t)M_3(0)=S(0,t) \\ a_1(t)N_1(0)+a_2(t)N_2(0)+a_3(t)N_3(0)=SH(0,t) \end{cases}}$$

Buongiorno Nardelli B., Santoleri R., *JTECH* 2005.
Buongiorno Nardelli B. et al., *JGR* 2006.
Buongiorno Nardelli B. et al., *Ocean Sci*.2012.
Buongiorno Nardelli B., *JGR*, 2013.

Validation of the 3D reconstructions

Mixed layer depth difference vs ARGO

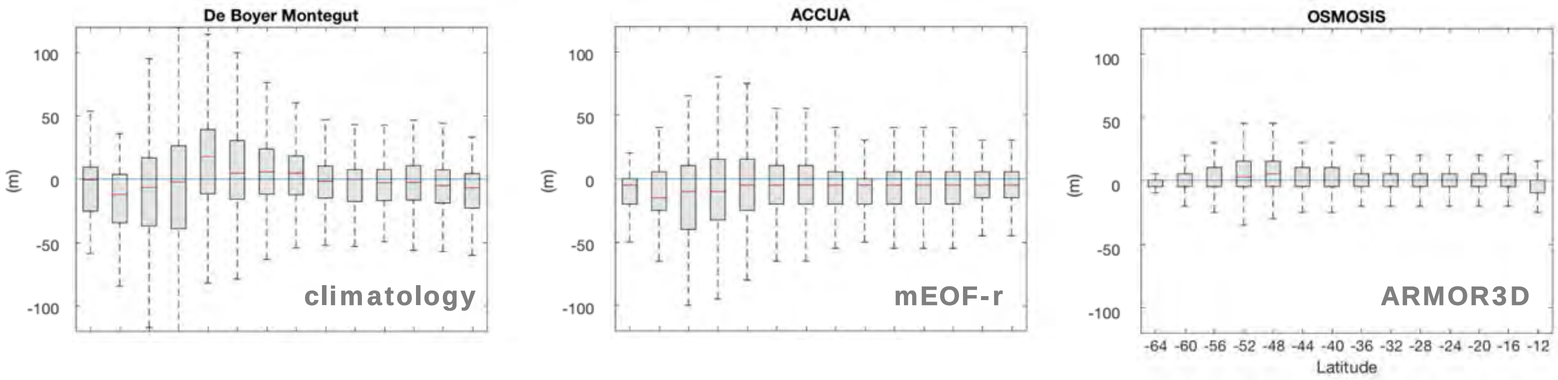

Differences reduced with respect to ***De Boyer Montégut*** *climatology*

3D reconstruction of the geostrophic currents from the thermal wind equation: the SURCOUF3D product (Mulet et al, 2014)

Altimetry :
Field of absolute geostrophic surface currents - weekly - 1/4°

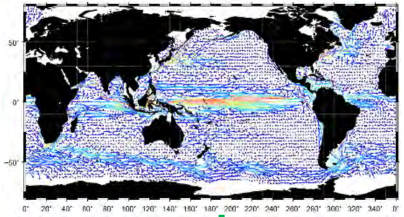

Armor3D :
3D T/S fields
weekly - 1/4° - [0-1500]m

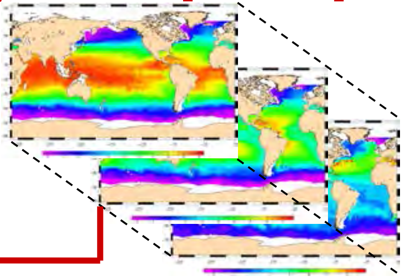

$$u(z=z_i) = u(z=0) + \frac{g}{\rho f}\int_{z=0}^{z_i} \frac{\partial}{\partial y}\rho'(z)\,dz$$

$$v(z=z_i) = v(z=0) - \frac{g}{\rho f}\int_{z=0}^{z_i} \frac{\partial}{\partial x}\rho'(z)\,dz$$

Guinehut et al, 2012

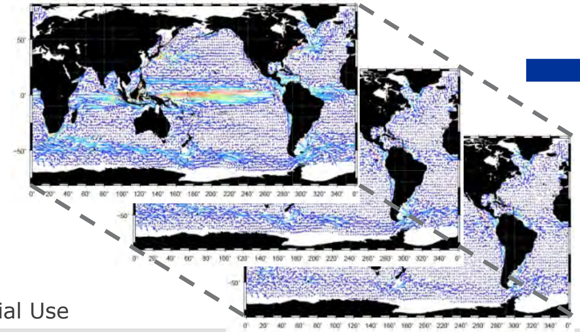

Surcouf3D
3D geostrophic current fields
weekly (1993-2018)
1/4° - 24 levels from 0 to1500m

Mulet et al, 2012

Surcouf3D - Comparison with model outputs

❑ Vertical section at 60°W, in 2006

Surcouf3D at 500m

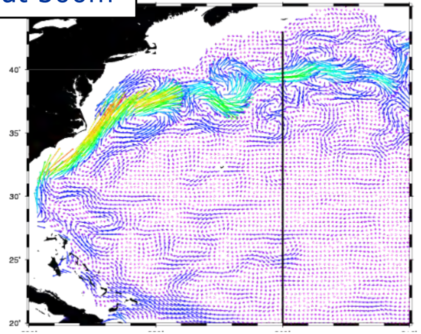

GLORYS at 500m

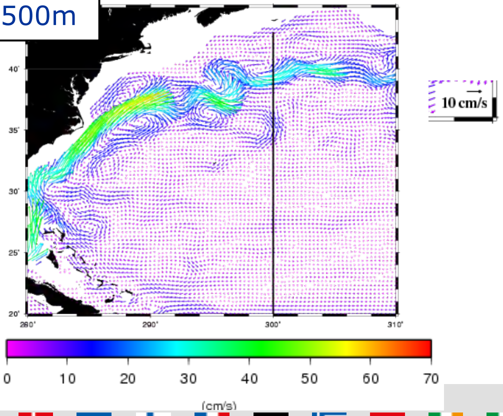

*geost. current with level of no motion at 1500m

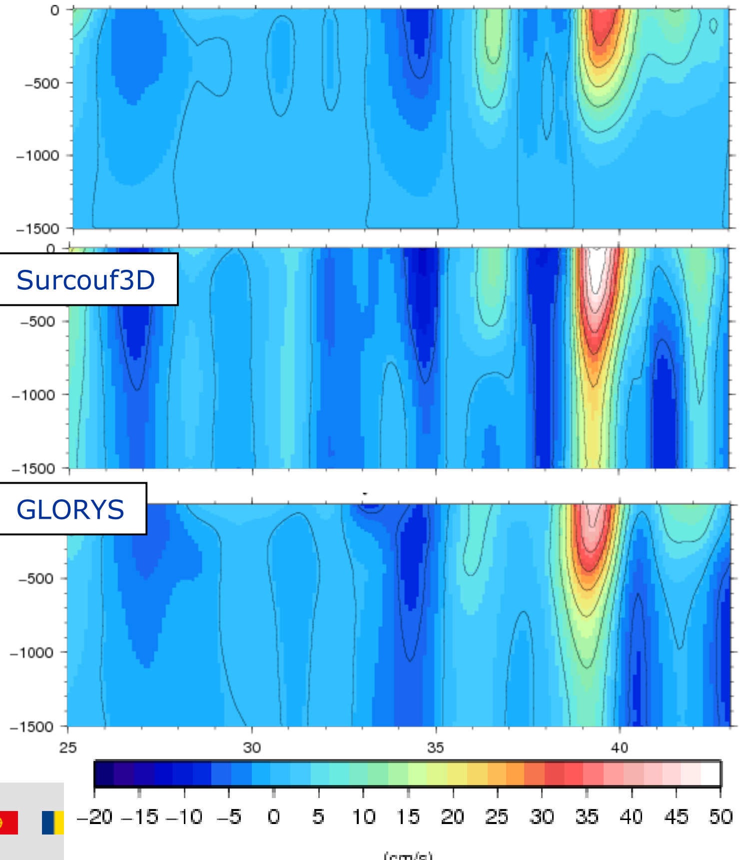

❑ Global statistics over the Atlantic outside the equateur (10°S-10°N)

Comparison between 3 different methods (**Surcouf3D**, **GLORYS**, **Armor3D**) and in-situ observations (**ANDRO**) at **1000 m** over the **2006/2007 period** (Taylor, 2001)

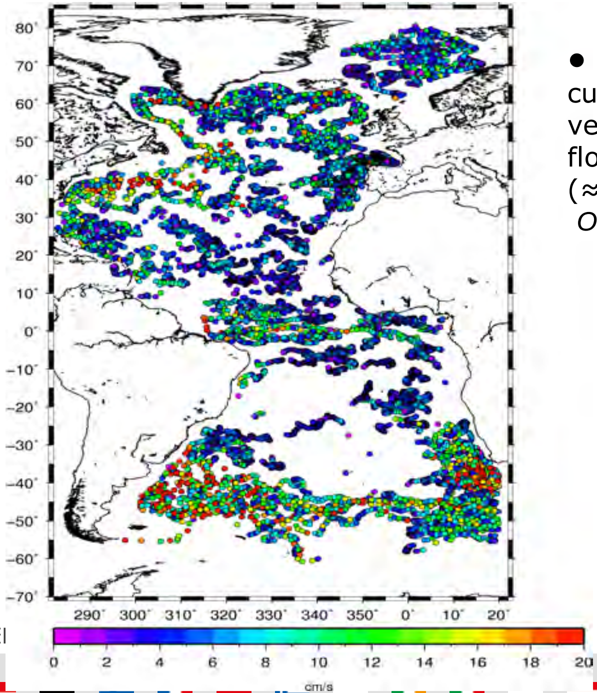

- **ANDRO** = 1000-m currents from drifting velocities from the Argo floats (≈10days, ≈50/100km)
  Ollitraut et al, 2010

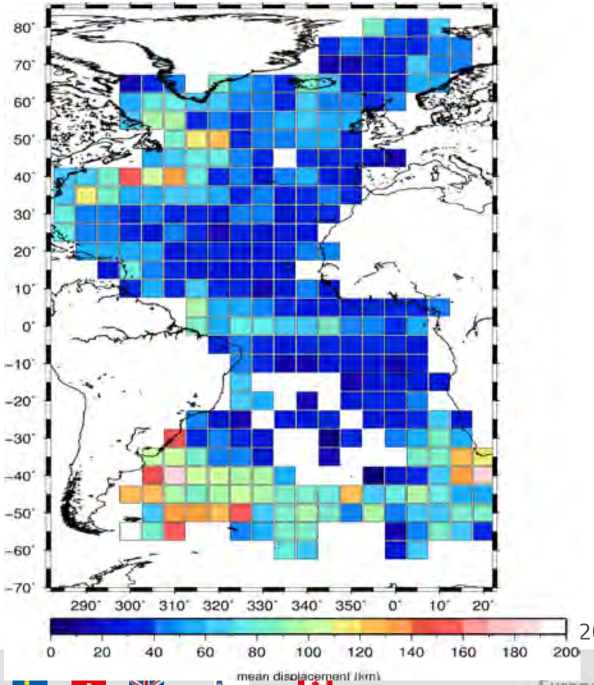

Surcouf3D - Validation of 1000-m currents

- Global statistics over the Atlantic outside the equateur (10°S-10°N)
  Comparison between 3 different methods (**Surcouf3D**, **GLORYS**, **Armor3D**) and in-situ observations (**ANDRO**) at **1000 m** over the **2006/2007 period** (Taylor, 2001)

Meridional component

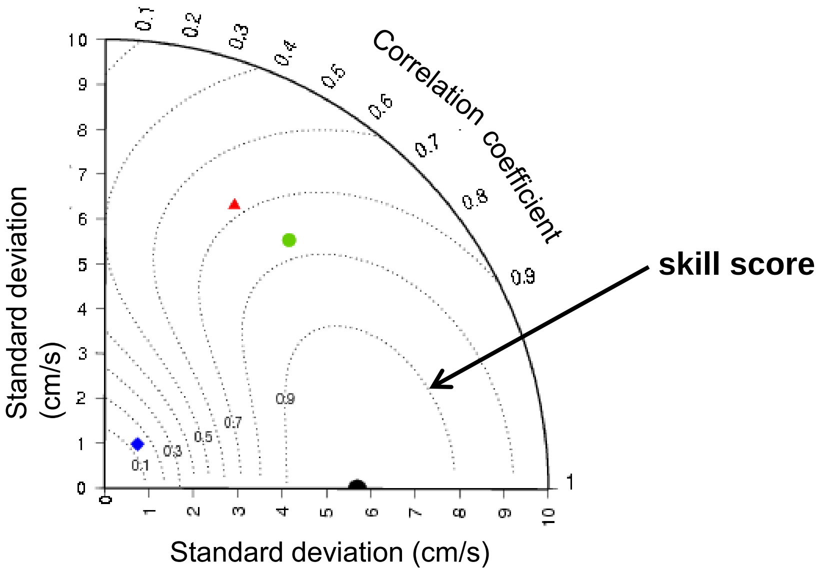

- **SURCOUF3D** (weekly, 1/3°)
- ▲ **GLORYS** = Mercator-Ocean reanalysis (weekly, 1/4°) *Ferry et al., 2010*
- ♦ **Armor3D** = geostrophic current with level of no-motion at 1500m (weekly, 1/3°)
- **ANDRO** = 1000-m currents from drifting velocities from the Argo floats (≈10days, ≈50/100km) *Ollitraut et al, 2010*

➔ Results are very **similar** for the **zonal component**

Comparison to YOMAHA velocities at 1000m for the period 1998-2015

Zonal bias at 1000m depth

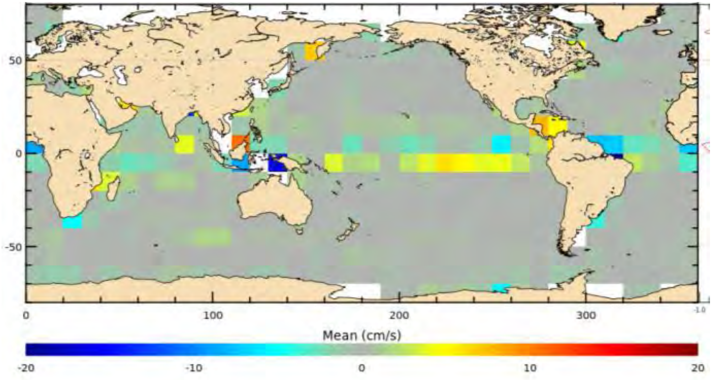

Meridional bias at 1000m depth

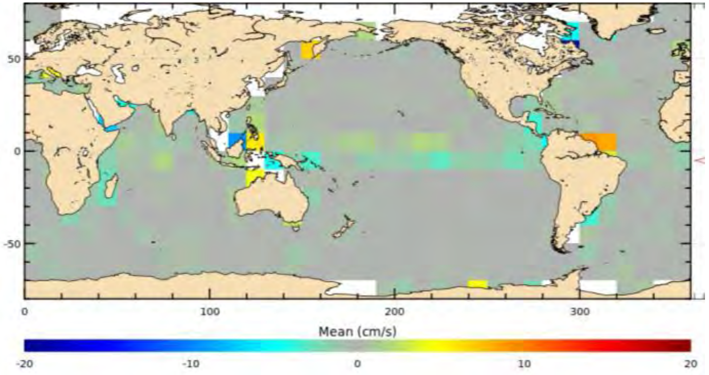

Zonal RMS at 1000m depth

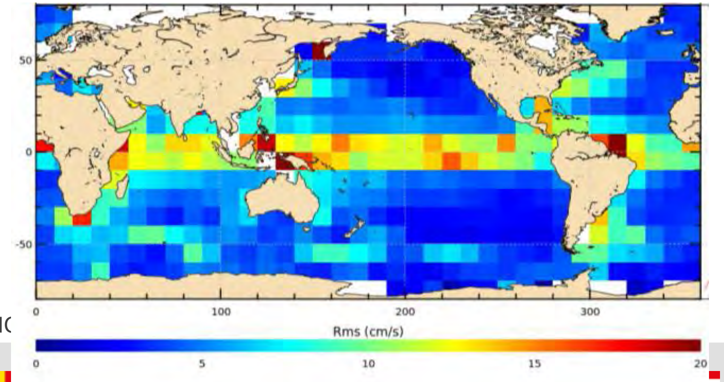

Meridional RMS at 1000m depth

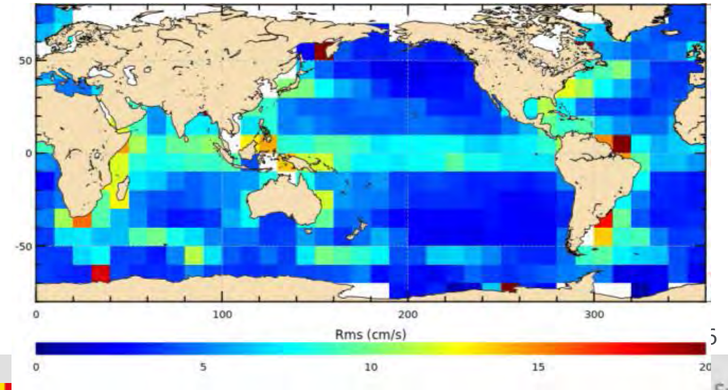

Surcouf3D - Validation

- Comparison with **GoodHope** **VM-ADCP observations** from 14/02–17/03/2008

SURCOUF3D
ADCP

Agulhas Rings

Subantarctic front

Polar front

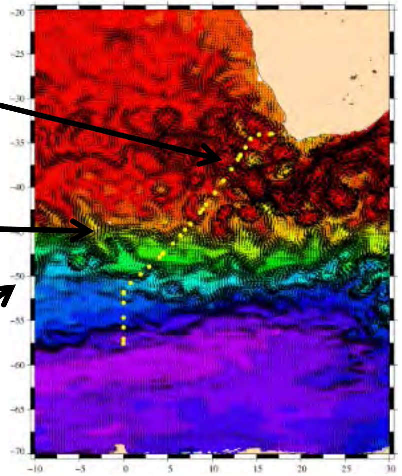

ADCP obs courtesy of S. Speich

Zonal velocities (cm / s)

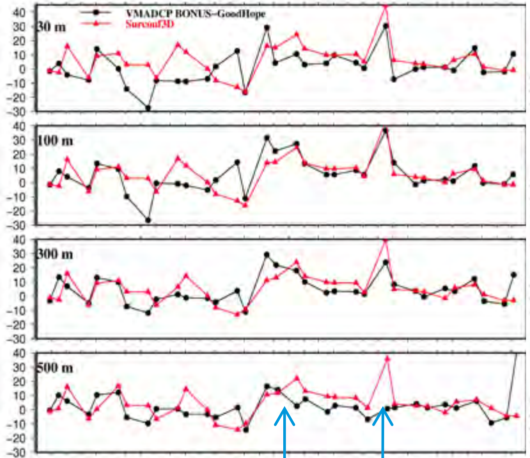

Meridional velocities (cm / s)

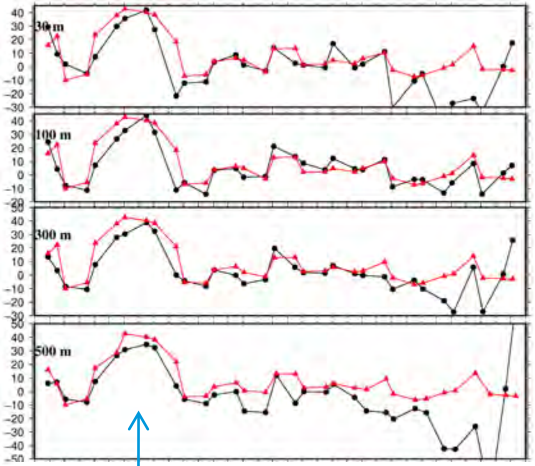

14 / 02 / 08

17 / 03 / 2008

Subantarctic front

Polar front

Agulhas Rings

➔ Good correlation with independent in-situ obs.

Surcouf3D - Validation

❑ Comparison with **RAPID current-meters** in the Western boundary current off the Bahamas from April 2004 to April 2005

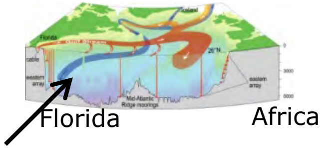

26.5°North
76.5°West

SURCOUF3D
RAPID (current meters)
GLORYS

➔ Good correlation with independent obs., and with GLORYS
➔ Importance of in-situ T/S profiles obs at depth for the inversion of the current

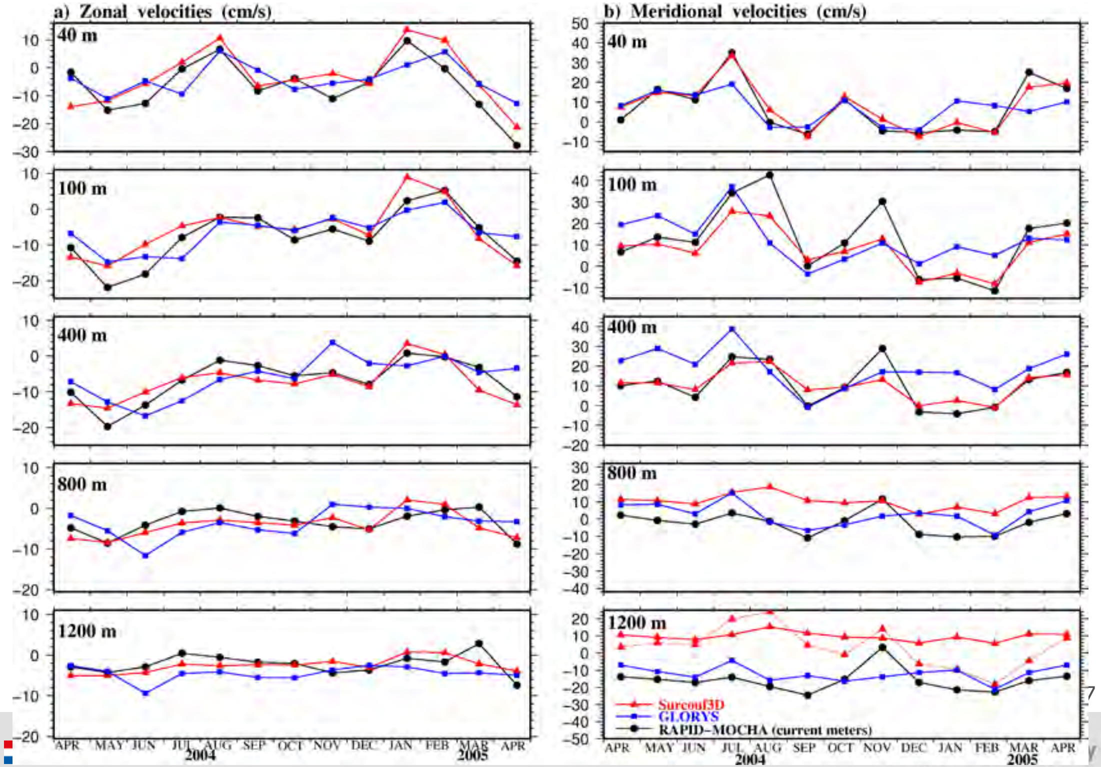

❑ Comparison with Bryden et al, 2005 (section at 24.5° from Africa to 73°W and at 26.5°N off Bahamas)

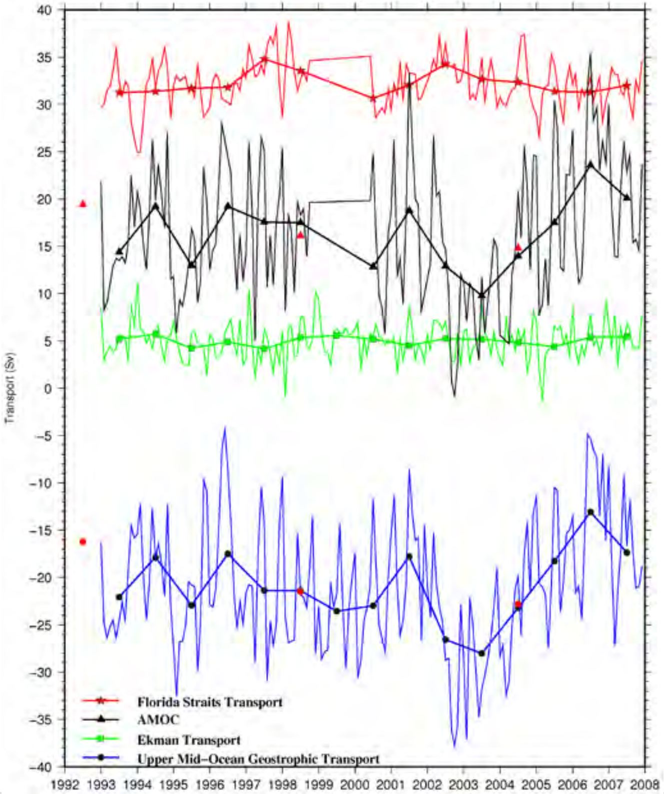

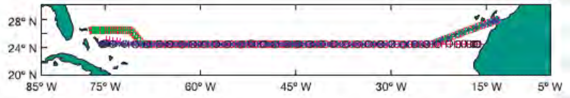

(Bryden et al,2005)

Floride Strait Transport
from electrical cable

AMOC = Geost + Ekman + Florida
(**Surcouf3D**, **Bryden et al., 2005**)

Ekman Transport from wind stress ERA Interim

Geostrophic Transport **from 75°W to 15°W** and **from the surface to 1000m** (**Surcouf3D**, **Bryden et al., 2005**)

➔Consistent with Bryden et al, 2005
➔Hight inter-annual variability

Mulet et al, 2012

The vertical velocity component

Vertical motion in the ocean is important for ocean dynamics on a vast range of scales, from turbulence to the global overturning circulation.
It plays a key role in the exchange of heat, salt and biogeochemical tracers between the surface and deep ocean.

However, vertical velocities at the ocean mesoscale are several orders of magnitude smaller than corresponding horizontal flows, making their direct monitoring a still unsolved challenge.

3D reconstruction of the ageostrophic u_a,v_a,w currents: the Omega equation

Horizontal momentum equation $\frac{D_g U}{D_t} - f v_a = 0$ $\frac{D_g V}{D_t} + f u_a = 0$

Mass conservation equation $\frac{D_g \rho}{D_t} + w \frac{\partial \rho}{\partial z} = 0$

+ hydrostatic approximation ⇒ (1) $N^2 w = -\frac{1}{\rho_0} \frac{D_g}{Dt}\left(\frac{\partial P}{\partial z}\right)$

N is the Brunt-vaisala frequency $N = \sqrt{-\frac{g}{\rho}\frac{\partial \rho}{\partial z}}$

$$\frac{\partial(1)}{\partial x} \qquad \frac{\partial}{\partial x}(N^2 w) - f^2 \frac{\partial u_a}{\partial z} = 2\mathrm{f}\left(\frac{\partial V}{\partial x}\frac{\partial U}{\partial z} + \frac{\partial V}{\partial y}\frac{\partial V}{\partial z}\right)$$

$$\frac{\partial(1)}{\partial y} \qquad \frac{\partial}{\partial y}(N^2 w) - f^2 \frac{\partial v_a}{\partial z} = -2\mathrm{f}\left(\frac{\partial U}{\partial x}\frac{\partial U}{\partial z} + \frac{\partial U}{\partial y}\frac{\partial V}{\partial z}\right)$$

$$\frac{\partial u_a}{\partial x} + \frac{\partial u_a}{\partial y} + \frac{\partial w}{\partial z} = 0$$

Continuity of the total velocity field

$$\nabla^2{}_h (N^2 w) + f^2 \frac{\partial^2 w}{\partial z^2} = 2\nabla_h \cdot \boldsymbol{Q}$$

with

$$Q = \left[f\left(\frac{\partial V}{\partial x}\frac{\partial U}{\partial z} + \frac{\partial V}{\partial y}\frac{\partial V}{\partial z}\right), -f\left(\frac{\partial U}{\partial x}\frac{\partial U}{\partial z} + \frac{\partial U}{\partial y}\frac{\partial V}{\partial z}\right)\right]$$

Net primary production in the GulfStream sustained by quasi-geostrophic vertical exchanges

Pascual et al, 2015, GRL

Map of geostrophic surface currents derived from ARMOR3D data for September 2005. The color map corresponds to the monthly mean of net primary production (mg C m2 d1) for the same month.

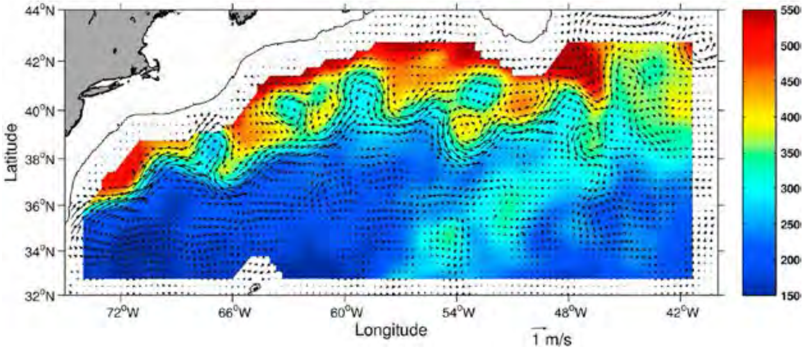

Intense vertical motion takes place along the jet, upstream/downstream of meander troughs, and within the mesoscale eddies, where multipolar vertical velocity patterns are generally observed.

Map of vertical velocity (m d^{-1}) at 100 m, obtained by integrating the QG omega equation from the 3-D field of ARMOR3D data corresponding to September 2005. Horizontal geostrophic currents are superimposed

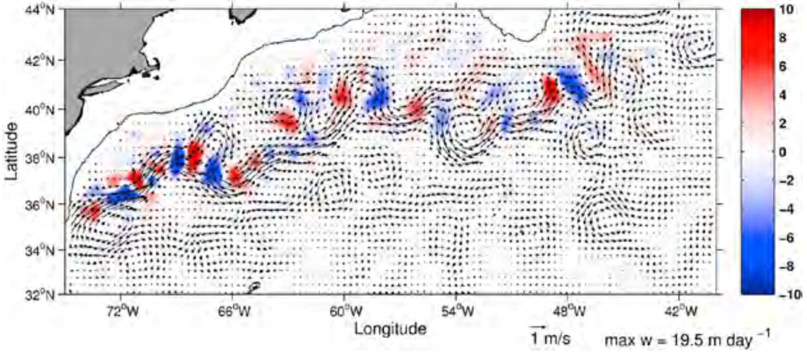

To first approximation, the dipoles of positive and negative vertical velocities around meanders are explained by conservation of potential vorticity [Pollard and Regier, 1992]

Application: Impact of vertical and horizontal advection on nutrient distribution in the southeast Pacific

Barcelo-Llull et al, 2016

- 12 years of vertical and horizontal currents are derived from ARMOR3D T/S field in the south-east Pacific.
- The impact of vertical velocity on nitrate uptake rates is assessed by using two Lagrangian particle tracking experiments that differ according to vertical forcing $w=w_{QG}$ vs $w=0$).
- vertical motions induce local increases in nitrate uptake reaching up to 30 %. Such increases occur in low uptake regions with high mesoscale activity. Despite being weaker than horizontal currents by a factor of up to 10^{-4}, vertical velocity associated with mesoscale activity is demonstrated to make an important contribution to nitrate uptake, hence productivity, in low uptake regions.

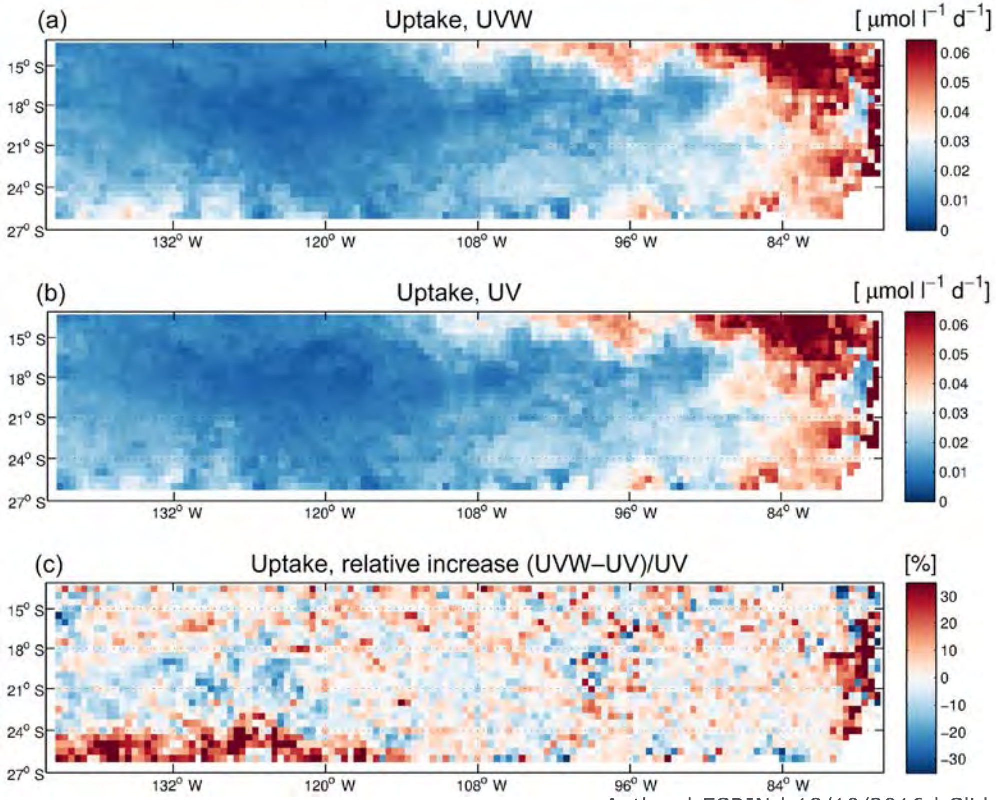

Estimating the net effect of mesoscale processes on Southern Ocean water mass formation

In Buongiorno et al (2018) more general formulations of the Omega equation are considered (in particular the Primitive Equation formulation and the semi-geostrophic formulation), also including the turbulent components of the Q vector (the effect of vertical mixing is introduced through a modified K-profile parameterization and using ERA-interim data)

Allowing to estimate separately:

- geostrophic/ageostrophic horizontal components
- Adiabatic (no heat exchange with surrounding waters) /diabatic vertical velocity components

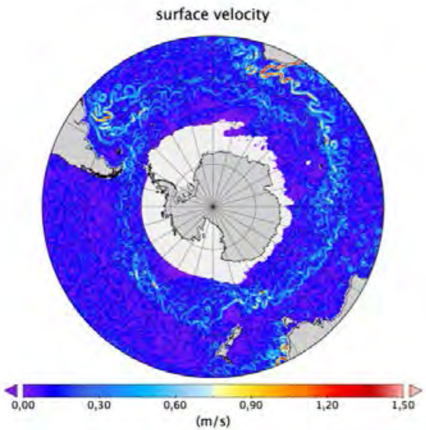

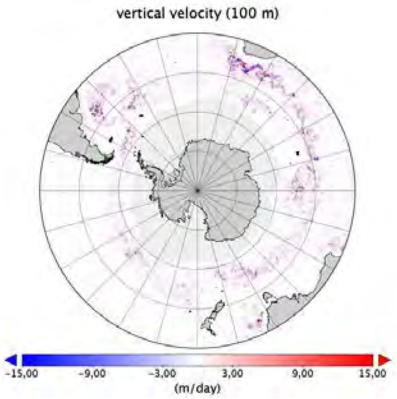

Estimating the net effect of mesoscale processes on Southern Ocean water mass formation

kinematic approach: evaluate the volume transport per water mass crossing the base of the winter mixed layer (Marshall et al., 1999)

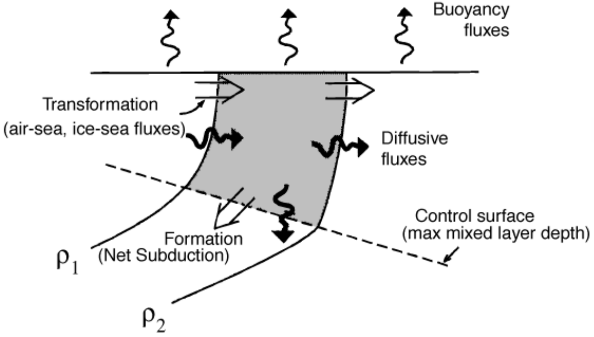

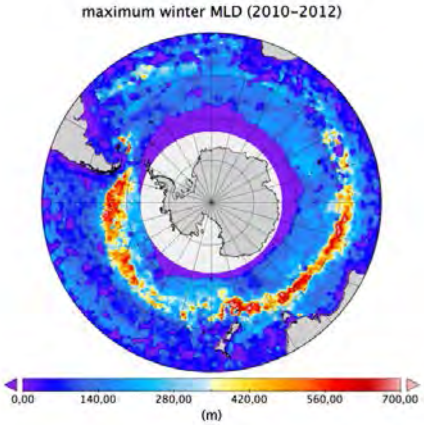

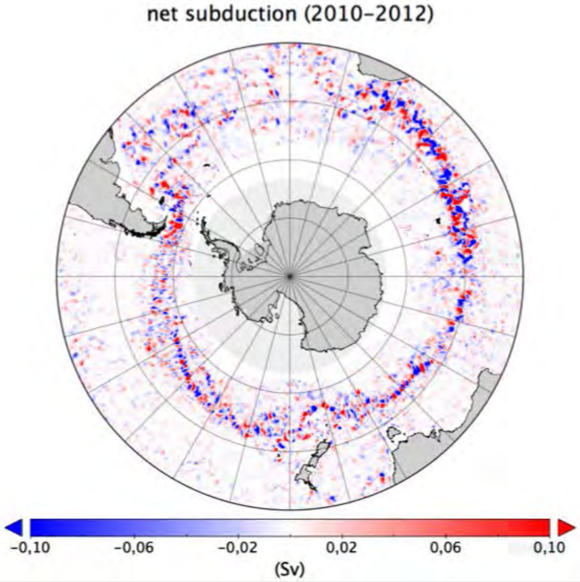

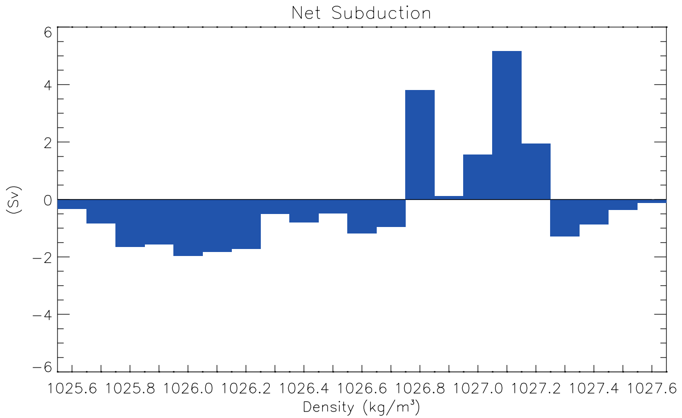

Estimating the net effect of mesoscale processes on Southern Ocean water mass formation

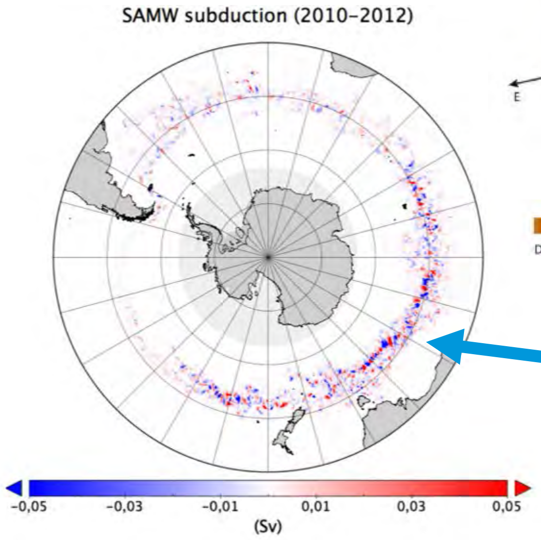

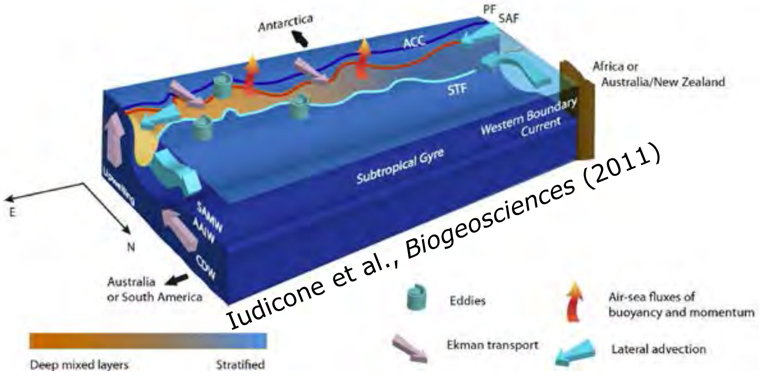

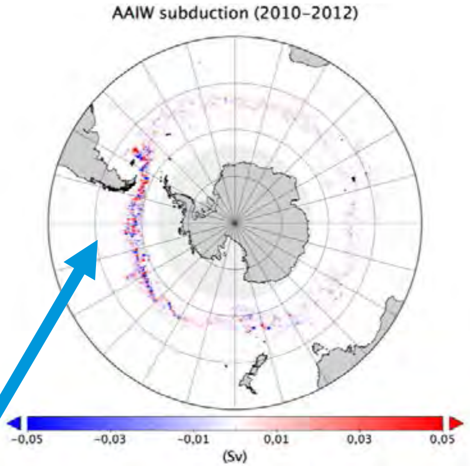

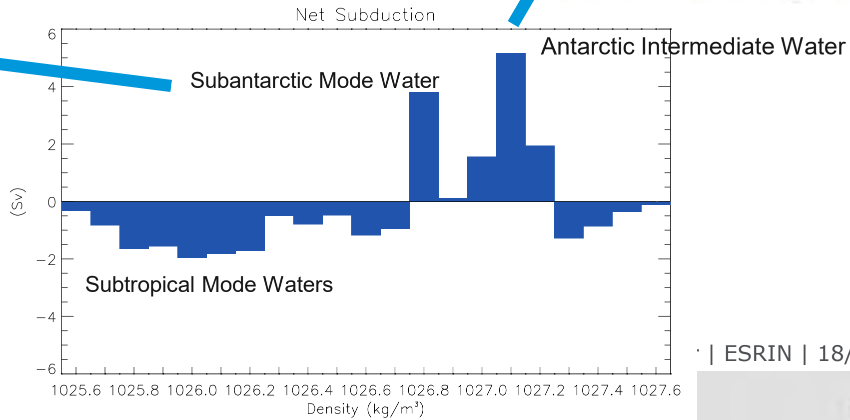

Estimating the net effect of mesoscale processes on Southern Ocean water mass formation

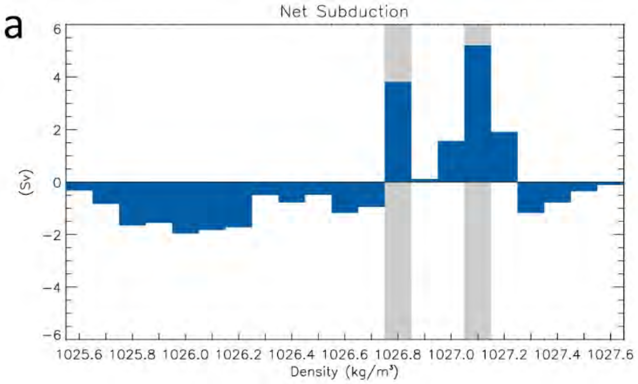

Impact of processes contributing to intermediate/mode water subduction can be analyzed separately:

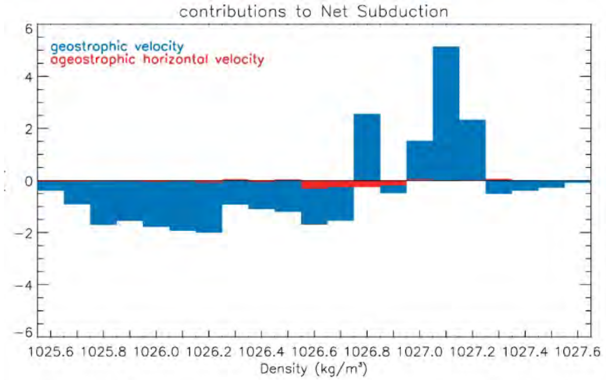

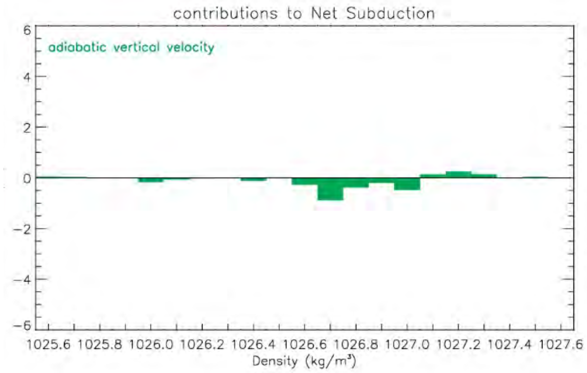

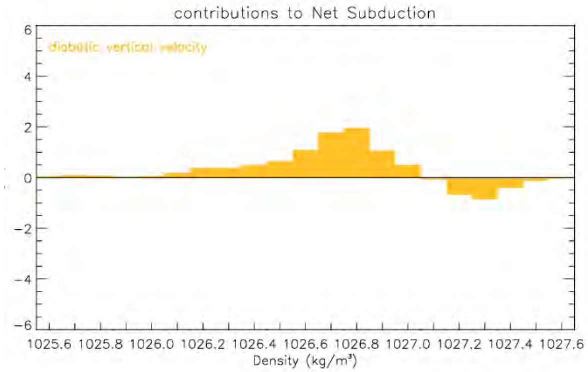

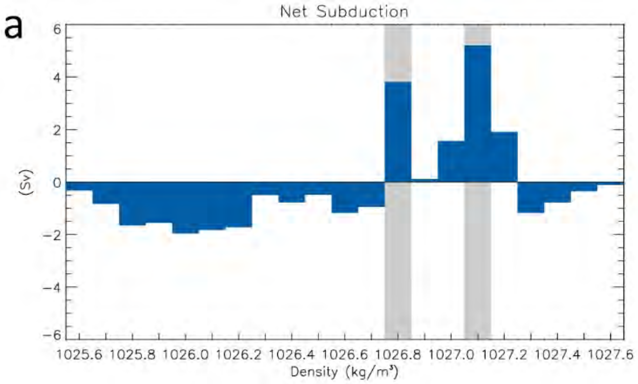

Impact of processes contributing to intermediate/mode water subduction can be analyzed separately:

Re-stratification driven by internal dynamics

Wind-driven downwelling

Wind-driven upwelling

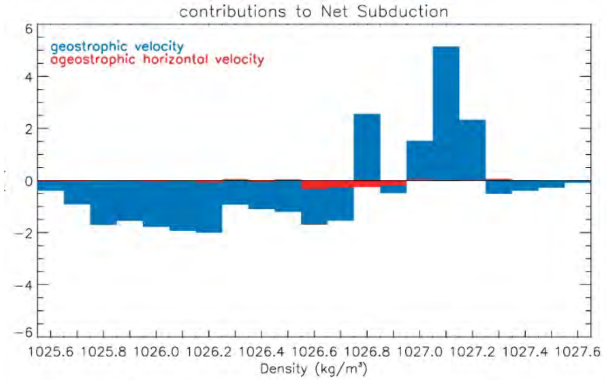

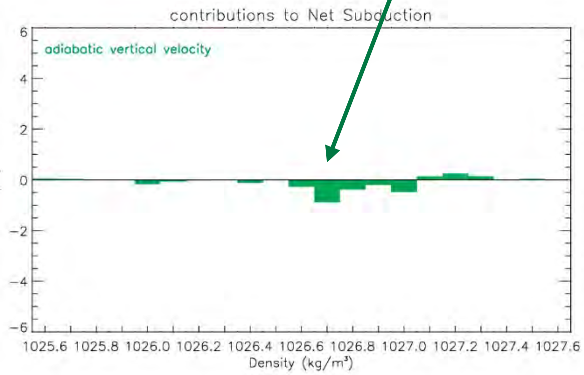

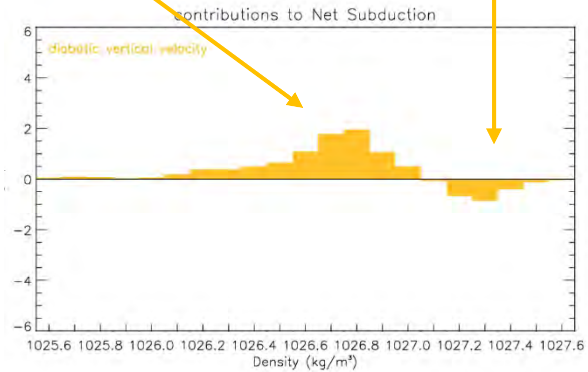

Estimating the net effect of mesoscale processes on Southern Ocean water mass formation

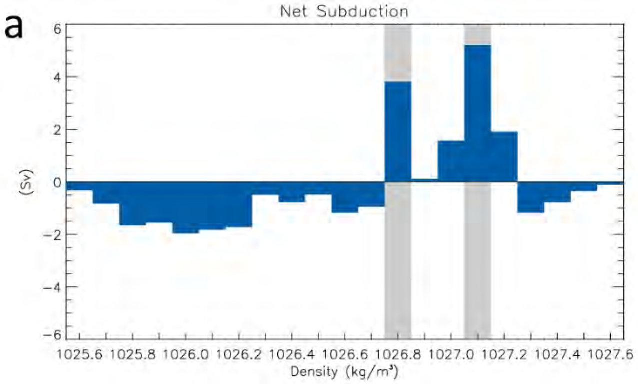

Impact of KPP mixing in Omega → similar to simple Ekman pumping/suction estimates